

# Multiconfiguration Dirac-Hartree-Fock calculations of transition rates and lifetimes of the eight lowest excited levels of radium

Jacek Bieroń<sup>1</sup>, Paul Indelicato<sup>2</sup>, and Per Jönsson<sup>3</sup>

<sup>1</sup> Instytut Fizyki imienia Mariana Smoluchowskiego  
Uniwersytet Jagielloński  
Reymonta 4, 30-059 Kraków, Poland  
e-mail: Bieron@uj.edu.pl

<sup>2</sup> Laboratoire Kastler Brossel, École Normale Supérieure  
CNRS; Université P. et M. Curie - Paris 6  
Case 74; 4, place Jussieu, 75252 Paris CEDEX 05, France  
e-mail: paul.indelicato@spectro.jussieu.fr

<sup>3</sup> Nature, Environment, Society  
Malmö University  
S-205 06 Malmö, Sweden  
e-mail: per.jonsson@ts.mah.se

**Abstract.** The multiconfiguration Dirac-Hartree-Fock (MCDHF) model has been employed to calculate the transition rates between the nine lowest levels of radium. The dominant rates were then used to evaluate the radiative lifetimes. The decay of the metastable  $7s7p^3P_0$  state through 2-photon E1M1 and hyperfine induced channels is also studied.

## 1 Introduction

Recent advances in trapping and spectroscopy of free, neutral atoms make it possible to extend the search for time reversal violation effects into the domain of radioactive elements [1]. In the last decade several heavy atoms were considered as candidates for experimental searches [2]. There are at least two ongoing atomic trap experiments (in Kernfysisch Versneller Instituut in Netherlands [3,4] and in Argonne National Lab in the U.S. [5,6]) whose aim is to detect the electric dipole moment of radium. The advantage of radium lies in octupole deformations of nuclei in several isotopes [7], simple electronic structure (ground state configuration  $[\text{Kr}]4d^{10}4f^{14}5s^25p^65d^{10}6s^26p^67s^2$  yields the closed-shell singlet state  $^1S_0$ ) as well as in coincidental proximity of two atomic states of opposite parity,  $7s7p^3P_1$  and  $7s6d^3D_2$ , which are separated by a very small energy interval  $5 \text{ cm}^{-1}$ .

The data on atomic spectrum of radium compiled in the tables of Moore [8] came from the experimental investigations of Rasmussen [9], with subsequent revisions by Russell [10]; both go back to the 1930s. These data cover only 69 classified lines. The isotope shifts and hyperfine structures of radium were measured by the group of Wendt [11,12,13,14,15,16] in the 1980s. They have studied both atomic Ra I and ionic Ra II spectra, and obtained the isotope shifts, magnetic dipole hyperfine constants  $A$  and electric quadrupole constants  $B$  of the  $7s7p^1P_1$ ,  $7s7p^3P_1$ ,  $7s7p^3P_2$ , and  $7s7d^3D_3$  levels of neutral radium, as well as the magnetic dipole hyperfine constants  $A$  of the  $7s^2S_{1/2}$ ,  $7p^2P_{1/2}$ , and  $7p^2P_{3/2}$  levels of  $\text{Ra}^+$  ion, together with the electric quadrupole constant  $B$  of the  $7p^2P_{3/2}$  state of  $\text{Ra}^+$ . Hyperfine structures of singly-ionised radium have been also the subject of several theoretical papers [17,18,19,20,21,22].

The excitation energies of several states of neutral and singly-ionised radium (and barium) were later calculated in the framework the relativistic coupled-cluster theory by the group of Kaldor [23,24]. More recently there have been three papers from our group in which we calculated the lifetimes of the  $7s7p\ ^1P_1$  and  $7s6d\ ^3D_2$  states [25]; the hyperfine structure constants of all levels belonging to the two lowest excited-state configurations [26]; and the electric field gradients generated by the electronic cloud in the  $7s7p\ ^1P_1$ ,  $7s7p\ ^3P_1$ , and  $7s7p\ ^3P_2$  states, which in turn (combined with the measured values of the electric quadrupole constants  $B$ ) yielded the nuclear electric quadrupole moment of radium-223 isotope [27]. The excitation energies and lifetimes of several states of radium (and barium) were calculated recently in the framework of the combined configuration-interaction and many-body perturbation theory by Dzuba and Ginges [28].

In the present paper we calculated the transition probabilities between the states arising from the three lowest configurations of radium:  $7s^2\ ^1S_0$ ,  $7s7p\ ^3P_{0,1,2}$ ,  $7s7p\ ^1P_1$ ,  $7s6d\ ^3D_{1,2,3}$ , and  $7s6d\ ^1D_2$ , as well as the lifetimes of these states. The purpose of the present paper is fourfold. Firstly, we intended to extend the transition rate calculations on all levels arising from the three lowest configurations (i.e.  $7s^2$ ,  $7s7p$ , and  $7s6d$ ). We included (1) transitions which contribute appreciably to lifetimes; (2) transitions involving  $7s6d\ ^3D_2$  and  $7s7p\ ^3P_1$  levels because they are of interest in EDM experiments (the mixing induced by T-odd interactions is strongest between these two levels); (3) transitions which may be important for trapping; (4) transitions which are stronger than  $1/s$  (a somewhat arbitrary threshold). Secondly, new comparison of our results became available when the two most recent papers [28,5] appeared in print. These in turn permitted further tests of the newly developed [29] parallel version of the GRASP package [30] and calibration the theoretical model for the calculations of the spectroscopic properties of radium. Finally, we present a summary of the available theoretical data on the spectroscopic properties of eight lowest excited levels of radium, with the hope that they may be of help for the experimental groups, that are currently in the process of setting up the atomic traps for the search of permanent electric dipole moments. The Argonne group has already measured [5] the frequency and the rate of the  $^3P_1 - ^1S_0$  transition in the  $^{225}\text{Ra}$  isotope, and determined the lifetime of the  $^3P_1$  level. The lifetime of this level have been previously calculated by Hafner and Schwarz [31] and by Bruneau [32].

## 2 Theory

The modified version [29] of the GRASP implementation [30] of the multiconfiguration Dirac-Hartree-Fock method [33] was used in the present paper. The starting point is the Dirac-Coulomb Hamiltonian

$$H_{DC} = \sum_i c\boldsymbol{\alpha}_i \cdot \mathbf{p}_i + (\beta_i - 1)c^2 + V_i^N + \sum_{i>j} 1/r_{ij}, \quad (1)$$

where  $V^N$  is the monopole part of the electron-nucleus Coulomb interaction. The wavefunction for a particular atomic state ( $\Psi$ ) is obtained as the self-consistent solution of the Dirac-Fock equation [30] in a basis of symmetry adapted configuration state functions ( $\Phi$ )

$$\Psi(\Gamma P J M) = \sum_i^{NCF} c_i \Phi(\gamma_i P J M). \quad (2)$$

The basis  $NCF$  was systematically enlarged [34,35] to yield increasingly accurate approximations to the exact wavefunction. All calculations were done with the nucleus modeled as a variable-density sphere, where a two-parameter Fermi function [36] was employed to approximate the charge distribution. The Breit and QED corrections were estimated with the step-wise procedure described in [34]. They were applied only to two transition rates, as explained in section 4.3 below.

### 3 Method

The wavefunctions were obtained with the active space method in which configuration state functions of a particular parity and symmetry are generated by substitutions from a reference configuration to an active set of orbitals. The active set and the multiconfiguration expansions are increased systematically. The whole process is governed by convergence of the expectation values. The calculations were divided into two stages. Each stage was further divided into several consecutive steps. In the first stage, the spectroscopic and virtual spinorbitals were generated in relatively small multiconfiguration expansions. The spectroscopic orbitals required to form a reference wavefunction were obtained with a minimal configuration expansion, with full relaxation. Then virtual orbitals were generated in five consecutive steps. At each step the virtual set has been extended by one layer of virtual orbitals. A layer is defined as a set of virtual orbitals with different angular symmetries. In the present paper five layers of virtual orbitals of each of the  $s$ ,  $p$ ,  $d$ ,  $f$ ,  $g$ ,  $h$  symmetries were generated. At each step the configuration expansions were limited to single and double substitutions from valence shells to all new orbitals and to all previously generated virtual layers. These were augmented by small subsets of dominant single and double substitutions from core and valence shells, with further restriction, that at most one electron may be promoted from core shells (which means, that in the case of a double substitution the second electron must be promoted from a valence shell). All configurations from earlier steps were retained, with all previously generated orbitals fixed, and all new orbitals made orthogonal to others of the same symmetry. The initial shapes of radial orbitals were obtained in Thomas-Fermi potential, and then driven to convergence with the self-consistency threshold set to  $10^{-8}$ . All radial orbitals were separately optimized for each of the nine atomic states of interest. The Optimal Level form of the variational expression [36] was applied in all variational calculations.

In the second stage, the configuration-interaction calculations (i.e., with no changes to the radial wavefunctions) were performed, with multiconfiguration expansions tailored in such a way, as to capture the dominant electron correlation contributions to the expectation values. The valence and core-valence effects constitute the dominant electron correlation contributions in the oscillator strength calculations [37], therefore all single and double substitutions were allowed from several core shells and both valence shells (i.e.,  $7s^2$ ,  $7s7p$ , or  $7s6d$ , depending on the state) to all virtual shells, with the same restriction as above, i.e. that at most one electron may be promoted from core shells. The virtual set was systematically increased from one to five layers, until the convergence of transition rates was obtained. In a similar manner, several core shells were systematically opened for electron substitutions — from the outermost  $6p$  to  $5s5p5d6s6p$  shells. The effects of substitutions from  $4s4p4d4f$  shells were neglected. We estimated them separately for three states and discovered that they change the calculated values of transition rates by no more than a fraction of a percent. The transition rates were calculated with the biorthonormal technique [38,39], which permits the application of standard Racah algebra, while retaining the advantage of wavefunctions separately optimized for each state. Experimental values of transition energies from Moore's tables [8] were used in calculations of transition rates.

## 4 Results

### 4.1 The metastable $7s7p^3P_0$ state

In principle there are three possible decay channels of the  $7s7p^3P_0$  state. It can decay to (the only lower lying) ground state through (1) a blackbody radiation induced decay, (2) a 2-photon E1M1 transition, or through (3) a hyperfine induced transition. The first is beyond the scope of the present paper, since it depends on the ambient temperature. Of the other two, the former can be estimated through an order-of-magnitude comparison with the E1M1  $1s2p^3P_0 - 1s^2^1S_0$  two-photon transition in helium-like heavy ions. We started from a recent evaluation [40], which gives  $3.14 \times 10^9 \text{ s}^{-1}$  for Ra. In order to obtain a good dependence on transition energy and radial matrix elements, we evaluated the E1M1 matrix elements (following Eq. (2) of Ref. [40])

for He-like Ra (using only  $1s2p\ ^3P_1$  as an intermediate state) and for neutral Ra (using only the  $7s7p\ ^3P_1$ ). Then we integrated over photon energies with the five-point Gauss-Legendre formula. Finally, we evaluated the ratio of these two values to scale the He-like E1M1 rate. This gives an order of magnitude estimate of  $9.6 \times 10^{-3} \text{ s}^{-1}$ . Such lifetime ( $\approx 100 \text{ s}$ ) of the  $7s7p\ ^3P_0$  state would be comparable to the lifetimes of nuclei of several radium isotopes (it would be significantly shorter only in comparison with the nuclei of the most stable radium isotopes spanning the mass range 223-229). This would be the case of spin-zero isotopes of radium.

For the isotopes of radium with a nonzero value of nuclear spin, the hyperfine-induced transition must also be considered. We estimated the  $7s7p\ ^3P_0 - 7s^2\ ^1S_0$  transition rate with a simple three-state model, in which the wavefunctions of the hyperfine components of the upper  $^3P_0$  state are described by a symmetry-adapted configuration-state-function expansion of the form

$$|7s7p\ ^3P_0 IF\rangle_{HFS} = c_0 |7s7p\ ^3P_0 IF\rangle + c_1 |7s7p\ ^1P_1 IF\rangle + c_2 |7s7p\ ^3P_1 IF\rangle \quad (3)$$

running over the appropriate hyperfine components  $IF$  of the  $^1P_1$  and  $^3P_1$  states. The hyperfine-induced transition rate (in  $\text{s}^{-1}$ ) may be approximately expressed as

$$A(7s7p\ ^3P_0^o \rightarrow 7s^2\ ^1S_0) = \frac{2.02613 \times 10^{18}}{3\lambda^3} \left| c_1 \langle 7s7p\ ^1P_1^o \| \mathbf{Q}_1^{(1)} \| 7s^2\ ^1S_0 \rangle + c_2 \langle 7s7p\ ^3P_1^o \| \mathbf{Q}_1^{(1)} \| 7s^2\ ^1S_0 \rangle \right|^2 \quad (4)$$

where  $\langle 7s7p\ ^1P_1^o \| \mathbf{Q}_1^{(1)} \| 7s^2\ ^1S_0 \rangle$  and  $\langle 7s7p\ ^3P_1^o \| \mathbf{Q}_1^{(1)} \| 7s^2\ ^1S_0 \rangle$  are reduced matrix elements for the electric dipole operator, and  $\lambda$  is the transition wavelength (in  $\text{\AA}$ ). The coefficients  $c_1$  and  $c_2$  are related to the off-diagonal magnetic dipole constants  $A_{M1}^{HFS}(^1P_1, ^3P_0)$  and  $A_{M1}^{HFS}(^3P_1, ^3P_0)$

$$c_1 = \sqrt{I(I+1)} \frac{A_{M1}^{HFS}(^1P_1, ^3P_0)}{\Delta E(^1P_1 - ^3P_0)}, \quad c_2 = \sqrt{I(I+1)} \frac{A_{M1}^{HFS}(^3P_1, ^3P_0)}{\Delta E(^3P_1 - ^3P_0)} \quad (5)$$

(see [41] or [42] for full derivation). The sum in the expansion (3) should run over all excited states, but the sum in Eq. (4) is usually dominated by those states, for which the transition rates to the ground state are large and at the same time the energy denominators in Eq. (5) are small. In case of the  $7s7p\ ^3P_0$  state of radium the  $7s7p\ ^3P_1$  and  $7s7p\ ^1P_1$  states dominate. The contribution of the reduced matrix element  $\langle 7s7p\ ^3P_1^o \| \mathbf{Q}_1^{(1)} \| 7s^2\ ^1S_0 \rangle$  is 3.7 times larger than that of the  $\langle 7s7p\ ^1P_1^o \| \mathbf{Q}_1^{(1)} \| 7s^2\ ^1S_0 \rangle$  matrix element. The contributions of other states are much smaller, due to the presence of the energy denominators in the coefficients (5) and to the fact that the corresponding off-diagonal matrix elements are many orders of magnitude smaller (actually they are exactly zero, unless non-orthogonality between fully relaxed wavefunctions and correlation effects are not neglected), and they can be safely ignored at present level of the overall accuracy. The rate of the hyperfine-induced transition is isotope-dependent, i.e. it depends on the nuclear spin and on the nuclear magnetic moment. As in our previous paper [27], the  $^{223}\text{Ra}$  isotope was chosen to set the nuclear parameters (the transition rate  $A(^3P_0 - ^1S_0)$  may be readily recalculated for other radium isotopes, for which nuclear spins and magnetic moments are known). The nuclear spin of  $^{223}\text{Ra}$  is  $I = 3/2$ , and the nuclear magnetic dipole moment  $\mu = 0.2705(19)\mu_N$  was taken from the paper of Arnold *et al* [13]. The electric dipole transition rates  $A(^1P_1 - ^1S_0)$  and  $A(^3P_1 - ^1S_0)$  from table 1 (in Babushkin gauge) were used. The off-diagonal magnetic dipole constants  $A_{M1}^{HFS}(^1P_1, ^3P_0) = 540 \text{ MHz}$ , and  $A_{M1}^{HFS}(^3P_1, ^3P_0) = 1172 \text{ MHz}$ , were evaluated with the use of the same wavefunctions, and in the same approximation, as described in section (3) above. Together they yield hyperfine-induced transition rate  $A(^3P_0 - ^1S_0) = 0.0210 \text{ s}^{-1}$  in case of constructive interference, and  $A(^3P_0 - ^1S_0) = 0.0070 \text{ s}^{-1}$  in case of destructive interference.

The above evaluations of the E1M1 and hyperfine-induced rates were performed independently. As it turned out, the two contributions are of the same size, therefore they have to be treated simultaneously. To this end we employed the effective Hamiltonian method [43]. It requires also an evaluation of the  $A_{M1}^{HFS}(^3P_1, ^1P_1)$  matrix element (851 MHz). The method is valid beyond the limits of the perturbation method exposed above, in particular it does not require that the energy separation between levels is large compared to level widths. It yields

$A(^3P_0 - ^1S_0) = 0.02935 \text{ s}^{-1}$  (if the two-photon transition is switched off the effective Hamiltonian method yields  $A(^3P_0 - ^1S_0) = 0.0197 \text{ s}^{-1}$ ). In the process of this calculation, we found out by comparison with the results of *mdfgme* code [44] that non-orthogonality between spinorbitals plays very important role in the evaluation of non-diagonal hyperfine matrix elements (neglecting it may even lead to a sign change). We employed a new code, developed by one of us (P.J.) to evaluate correlated off-diagonal hyperfine matrix elements from GRASP wavefunctions, taking into account the effect of non-orthogonality between spinorbitals.

The accuracy is limited by the electric dipole matrix elements  $\langle 7s7p \ ^3P_1^o \| \mathbf{Q}_1^{(1)} \| 7s^2 \ ^1S_0 \rangle$  and  $\langle 7s7p \ ^1P_1^o \| \mathbf{Q}_1^{(1)} \| 7s^2 \ ^1S_0 \rangle$  as well as by the off-diagonal magnetic dipole constants  $A_{M1}^{HFS}(^3P_1, ^1P_1)$ ,  $A_{M1}^{HFS}(^3P_1, ^3P_0)$  and  $A_{M1}^{HFS}(^1P_1, ^3P_0)$ . In case of the matrix element  $\langle 7s7p \ ^3P_1^o \| \mathbf{Q}_1^{(1)} \| 7s^2 \ ^1S_0 \rangle$  we may assume the 5% relative accuracy for the  $^3P_1 - ^1S_0$  transition rate from experiment [5]. The accuracy of the  $A(^1P_1 - ^1S_0)$  rate is more difficult to estimate (see ref. [25]). This is the strongest, 'allowed' transition in the radium spectrum, but (as mentioned above) the contribution of its matrix element  $\langle 7s7p \ ^1P_1^o \| \mathbf{Q}_1^{(1)} \| 7s^2 \ ^1S_0 \rangle$  to the total value of the calculated rate of the hyperfine-induced transition  $^3P_0 - ^1S_0$  is 3.7 times smaller than that of the  $\langle 7s7p \ ^3P_1^o \| \mathbf{Q}_1^{(1)} \| 7s^2 \ ^1S_0 \rangle$  matrix element, so even a relatively large error bar would be quenched. We may very conservatively take the entire difference between the Babushkin and Coulomb gauge final values from table 1 in reference [25] as the error limit, obtaining a relative accuracy 25% for the  $A(^1P_1 - ^1S_0)$  transition probability. The accuracy of the diagonal magnetic dipole constants was estimated to be 6% (see [26]). Since an off-diagonal constant depends on both states rather than on one, we, again quite conservatively, doubled the 'diagonal' error limit estimate and assumed 12% as the contributions of the off-diagonal hyperfine constants to the error bar. Eventually, the above procedure yields the lifetime of the metastable  $^3P_0$  state  $\tau = 34(15)s$  of  $^{223}\text{Ra}$  isotope. The lifetime is based on both the 2-photon and hyperfine-induced channels. The error bar does not include the 2-photon contribution.

## 4.2 The $7s7p \ ^3P_1$ state

Figure 1 presents the transition probability  $A(^3P_1 - ^1S_0)$  as a function of the size of the multiconfiguration expansion. The transition rates were calculated in Babushkin and Coulomb gauges, which in the non-relativistic formulation correspond to length and velocity form of the transition integral, respectively. Both curves were obtained in the 'core-valence' approximation described above. The resulting Babushkin and Coulomb values are compared with the experimental result obtained by the Argonne group [5] and with three available theoretical values (the value  $A=4 \cdot 10^6 \text{ s}^{-1}$  obtained by Bruneau [32] did not fit within the vertical scale of figure 1). It is clearly seen in the figure 1 that the core-valence correlation effects are saturated in the framework of the single and restricted double substitutions and five layers of virtual orbitals, as described in section (3) above. The remaining difference between the final Babushkin and Coulomb gauge values may be attributed to the omitted core-core effects. We have made an attempt to estimate the contribution of the core-core correlation to  $^3D_2 - ^1S_0$  and  $^1P_1 - ^1S_0$  transition rates [25], but for other transitions the gauge differences and comparisons with data obtained by other authors, where available, are the only indications of the accuracy of our calculated rates. Although the gauge difference must not be treated as the error bar per se, it is a useful indicator in partially saturated multiconfiguration calculations of transition rates. The values obtained in the Babushkin gauge are weighted toward the outer parts of the electronic wavefunctions, while the Coulomb gauge values weight more inner parts, where the core-core effects arise. Therefore partially saturated expansions often produce Babushkin and Coulomb gauge values converging toward different limits, as in figure 1, with the difference arising from the omitted core-core effects. This is also the reason why Babushkin gauge results are usually treated as more reliable, which seems to be confirmed by the agreement of the Babushkin gauge transition rate  $A(^3P_1 - ^1S_0)$  with experiment (although agreement this close is very likely accidental; and good agreement for one level is not enough to justify a more general rule).

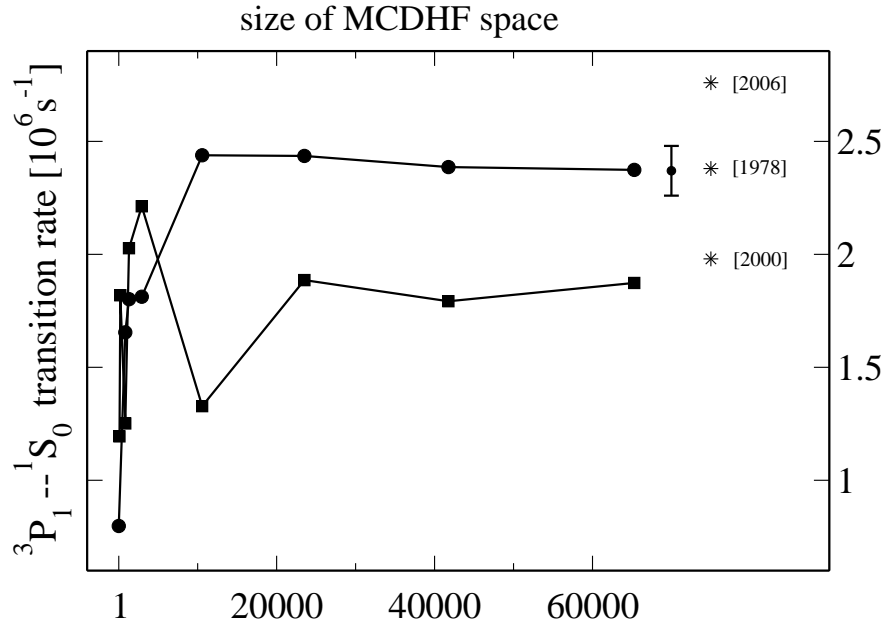


**Fig. 1.** Transition probability  $A(^3P_1 - ^1S_0)$  in Babushkin (upper curve with circles) and Coulomb (lower curve with squares) gauges, as a function of the multiconfiguration expansion (in core-valence approximation — see text for details). The lone dot with error bars (to the right from the end of the Babushkin curve) represents the experimental result from reference [5]. The three stars at the far right represent the theoretical data obtained by other authors and are denoted by publication year in brackets: [1978] — reference [31]; [2000] — reference [45]; [2006] — reference [28].

### 4.3 The $7s6d\ ^3D_2$ and $7s7p\ ^1P_1$ states

These two levels are distinguished because they were the subject of a separate paper [25]. In the present paper we duly quote the data obtained in core-valence approximation, and the reader is referred to the above mentioned paper for further discussion.

### 4.4 The remaining $7s7p\ ^3P_2$ , $7s6d\ ^3D_1$ , $7s6d\ ^3D_3$ , and $7s6d\ ^1D_2$ states

The remaining  $7s7p\ ^3P_2$ ,  $7s6d\ ^3D_1$ ,  $7s6d\ ^3D_3$ , and  $7s6d\ ^1D_2$  states, together with the states discussed in sections 4.1, 4.2, and 4.3 above, constitute full set of states arising from the three lowest electronic configurations of radium.

Some of these levels should also be considered metastable, not only  $7s7p\ ^3P_0$ . The  $^3D_3 - ^3D_2$  transition is the strongest 'direct' decay channel for the  $^3D_3$  state, but it is in fact very weak (comparable to that of the  $^3P_0 - ^1S_0$  transition). The rates of other possible 'direct' decay channels would be still smaller (e.g. M2 transition  $^3D_3 - ^3P_1$  rate is comparable to that of the  $^3D_2 - ^3P_0$  transition), therefore the multiphoton or hyperfine-induced transitions may also play a role in the  $^3D_3$  lifetime. Similar considerations may in principle apply to the  $^3P_2$ ,  $^1D_2$ , and  $^3D_2$  states (we did not pursue this issue, though).

## 5 Summary and conclusions

Table 1 presents calculated transition rates, and the lifetimes are presented in table 2. Coulomb gauge values of electric multipole transitions from the table 1 were not used to obtain the lifetimes. With the exception of the  $^3P_0$  level, the transition rates are given with 4 significant digits and the lifetimes with 3 significant digits, but that not necessarily reflects their accuracy.

**Table 1.** Calculated transition rates between nine lowest levels of radium [ $s^{-1}$ ]. Transition multiplicities are denoted by E1, E2, M1, M2; the Babushkin and Coulomb gauge values by (B) and (C), respectively. HFS means hyperfine-induced. Numbers in brackets represent powers of 10.

transition	This work	Ref. [28]	Expt. [5]
$^3P_0 - ^1S_0$ HFS+E1M1	2.935[-2]		
$^3P_1 - ^1S_0$ E1(B)	2.374[6]	2.760[6]	2.37(12)[6]
(C)	1.873[6]		
$^3P_1 - ^3P_0$ M1	1.334[-2]		
$^3P_1 - ^3D_1$ E1(B)	8.794[1]	9.850[1]	
(C)	4.025[3]		
$^3P_1 - ^3D_2$ E1(B)	1.775[-3]	1.572[-3]	
(C)	1.607[2]		
$^3P_2 - ^3P_0$ E2(B)	1.185[-2]		
(C)	1.243[-2]		
$^3P_2 - ^3D_1$ E1(B)	4.310[3]	4.897[3]	
(C)	9.722[3]		
$^3P_2 - ^3D_2$ E1(B)	4.602[4]	5.204[4]	
(C)	1.109[5]		
$^3P_2 - ^3D_3$ E1(B)	1.044[5]	1.234[5]	
(C)	4.201[5]		
$^1P_1 - ^1S_0$ E1(B)	1.793[8]	1.805[8]	
(C)	1.795[8]		
$^1P_1 - ^3D_1$ E1(B)	3.282[4]	4.195[4]	
(C)	5.222[4]		
$^1P_1 - ^3D_2$ E1(B)	9.793[4]	2.646[4]	
(C)	1.441[5]		
$^1P_1 - ^1D_2$ E1(B)	3.241[5]	3.194[5]	
(C)	5.875[5]		
$^3D_1 - ^3P_0$ E1(B)	1.390[3]	1.529[3]	
(C)	7.940[3]		
$^3D_2 - ^1S_0$ E2(B)	2.524[-1]	3.032[-1]	
(C)	1.630[-1]		
$^3D_2 - ^3P_0$ M2	3.021[-13]		
$^3D_2 - ^3D_1$ M1	5.082[-4]		
$^3D_3 - ^3D_2$ M1	6.352[-3]		
$^1D_2 - ^1S_0$ E2(B)	2.710[1]		
(C)	2.271[1]		
$^1D_2 - ^3P_1$ E1(B)	6.960[2]	7.722[3]	
(C)	1.224[3]		
$^1D_2 - ^3P_2$ E1(B)	5.930[0]	7.973[0]	
(C)	7.535[0]		

As discussed in section (4.2) above, the accuracy of our results is difficult to estimate, but it is probably much worse than 3 or 4 digits, particularly for very weak transitions.

The results of the present calculations may be considered as fully converged in core-valence approximation (convergence has indeed been observed for all transitions, similarly to that shown in figure 1), with core-core effects omitted.

With the exception of the  $^1P_1 - ^3D_2$  and  $^1D_2 - ^3P_1$  transitions (we cannot offer any plausible explanation for these discrepancies), our Babushkin gauge values are in reasonably good agreement with the results of Dzuba and Ginges [28]. An interesting feature is the large discrepancy between the results obtained in Babushkin and Coulomb gauges for transitions connecting closely-lying triplet  $P$  and triplet  $D$  states. The B/C ratios (i.e. the ratios of Babushkin versus Coulomb gauge results) turned out to be much closer to unity for those transitions when the experimental energies in the transition operator were replaced by theoretical ones. This observation, together with inconsistent results of the calculations of energies of excited states, had led

**Table 2.** Calculated lifetimes of eight lowest excited states of radium, compared with data from other authors.

state	This work	Ref. [28]	Ref. [45]	Ref. [31]	Ref. [32]	Expt. [5]
$^3P_0$	34(15) s <sup>a</sup>					
$^3P_1$	421 ns	362 ns	505 ns	420 ns	250 ns	422(20) ns
$^3P_2$	6.46 $\mu$ s	5.55 $\mu$ s	5.2 $\mu$ s			
$^1P_1$	5.56 ns	5.53 ns	5.5 ns			
$^3D_1$	719 $\mu$ s	654 $\mu$ s	617 $\mu$ s			
$^3D_2$	3.95 s	3.3 s	15 s			
$^3D_3$	157 s <sup>b</sup>					
$^1D_2$	1.37 ms	0.129 ms <sup>c</sup>	38 ms			

(a) based on E1M1 and hfs-induced decay channels in the  $^{223}_{88}\text{Ra}$  isotope

(b) based on  $^3D_3 - ^3D_2$  magnetic dipole transition only; other possible decay channels neglected

(c) calculated from transition probabilities quoted after Table VI in Ref. [28]

us [25] to suggest an experimental verification of radium data in Moore's tables [8]. At that time we were not aware of the papers by Eliav *et al* [23] and Landau *et al* [24], where the excitation energies of radium were calculated in the coupled-cluster approximation. More recently these calculations were independently confirmed within the framework of the CI+MBPT theory [28]. In both cases good agreement with experiment had been achieved. There are two principal differences between the methods and approximations used in the abovementioned three papers with respect to the methods and approximations used in the present paper. The transition rates were the primary targets of the present calculations, not the transition energies. Therefore we optimised the electronic wavefunctions separately for each of the nine states of interest. The core-valence correlation effects were fully accounted for. The core-core correlation effects, which are less important in calculations of transition rates and hyperfine structures, were treated in a very crude approximation in the cases of  $^1S_0$ ,  $^3D_2$  and  $^1P_1$  states, and were neglected for other states. The calculations of energy level differences require well balanced orbital sets and extensive multiconfiguration expansions. The results are usually in better agreement with experiment if a common set of orbitals is used for both states. If the orbital sets are separately optimised, the transition energy is obtained as a pure difference of the total energies of the two states of interest. They are both several orders of magnitude (five orders in case of radium) larger than the transition energy itself, therefore our calculated transition energy values may be less accurate than the calculated transition rates and hyperfine structures. Any further refinement of the present calculations would require computer resources, which are currently unavailable.

## 6 Acknowledgments

This work was supported by the Polish Ministry of Science and Higher Education (MNiSW) in the framework of the scientific grant No. 1 P03B 110 30 awarded for the years 2006-2009.

Laboratoire Kastler Brossel is Unité Mixte de Recherche du CNRS n° C8552.

P.J. acknowledges the support from the Swedish Research Council (VR).

## References

1. J.A. Behr, A. Gorelov, D. Melconian, M. Trinczek, W.P. Alford, D. Ashery, P.G. Bricault, L. Courneyea, J.M. D'Auria, J. Deutsch *et al.*, *Eur. Phys. J. A* **25**, 685 (2005)
2. J.S.M. Ginges, V.V. Flambaum, *Phys. Rep.* **397**, 63 (2004)
3. K. Jungmann, *Acta Phys. Pol. B* **33**, 2049 (2002)
4. URL [www.kvi.nl/trimp/web/html/trimp.html](http://www.kvi.nl/trimp/web/html/trimp.html)
5. N.D. Scielzo, J.R. Guest, E.C. Schulte, I. Ahmad, K. Bailey, D.L. Bowers, R.J. Holt, Z.T. Lu, T.P. O'Connor, D.H. Potterveld, *Phys. Rev. A* **73**, 010501(R) (2006)



6. URL [www-mep.phy.anl.gov/atta/research/radiumedm.html](http://www-mep.phy.anl.gov/atta/research/radiumedm.html)
7. J. Engel, Eur. Phys. J. A **25**, 691 (2005)
8. C.E. Moore, *Atomic Energy Levels*, NSRDS-NBS No 35, (Washington DC: US Govt. Printing Office) (1971)
9. E. Rasmussen, Z. Phys. **87**, 607 (1934)
10. H.N. Russell, Phys. Rev. **46**, 989 (1934)
11. S.A. Ahmad, W. Klempt, R. Neugart, E.W. Otten, K. Wendt, C. Ekström, ISOLDE Collaboration, Phys. Lett. **133B**, 47 (1983)
12. K. Wendt, S.A. Ahmad, W. Klempt, R. Neugart, E.W. Otten, H.H. Stroke, Z. Phys. D — Atoms, Molecules and Clusters **4**, 227 (1987)
13. E. Arnold, W. Borchers, M. Carre, H.T. Duong, P. Juncar, J. Lerme, S. Liberman, W. Neu, R. Neugart, E.W. Otten et al., Phys. Rev. Lett. **59**, 771 (1987)
14. S.A. Ahmad, W. Klempt, R. Neugart, E.W. Otten, P.G. Reinhard, G. Ulm, K. Wendt, The ISOLDE Collaboration, Nucl. Phys. A **483**, 244 (1988)
15. W. Neu, R. Neugart, E.W. Otten, G. Passler, K. Wendt, B. Fricke, E. Arnold, H.J. Kluge, G. Ulm, The ISOLDE Collaboration, Z. Phys. D — Atoms, Molecules and Clusters **11**, 105 (1989)
16. R. Neugart, E.W. Otten, K. Wendt, S.A. Ahmad, S.N. Panigrahy, R.W. Dougherty, K.C. Mishra, T.P. Das, J. Andriessen, Hyp. Int. **59**, 145 (1990)
17. V.A. Dzuba, V.V. Flambaum, O.P. Sushkov, Phys. Scr. **32**, 507 (1985)
18. J.L. Heully, A.M. Mårtensson-Pendrill, Phys. Scr. **31**, 169 (1985)
19. S.N. Panigrahy, R.W. Dougherty, S. Ahmad, K.C. Mishra, T.P. Das, J. Andriessen, R. Neugart, E.W. Otten, K. Wendt, Phys. Rev. A **43**, 2215 (1991)
20. J. Andriessen, H. Postma, A.M. van den Brink, Phys. Rev. A **45**, 1389 (1992)
21. X. Yuan, S.N. Panigrahy, R.W. Dougherty, T.P. Das, J. Andriessen, Phys. Rev. A **52**, 197 (1995)
22. X. Yuan, R.W. Dougherty, T.P. Das, J. Andriessen, Phys. Rev. A **52**, 3563 (1995)
23. E. Eliav, U. Kaldor, Phys. Rev. A **53**, 3050 (1996)
24. A. Landau, E. Eliav, U. Kaldor, J. Chem. Phys. **113**, 9905 (2000)
25. J. Bieroń, C. Froese Fischer, S. Fritzsche, K. Pachucki, J. Phys. B: At. Mol. Opt. Phys. **37**, L305 (2004)
26. J. Bieroń, J. Phys. B: At. Mol. Opt. Phys. **38**, 2221 (2005)
27. J. Bieroń, P. Pyykkö, Phys. Rev. A **71**, 032502 (2005)
28. V.A. Dzuba, J.S.M. Ginges, Phys. Rev. A **73**, 032503 (2006)
29. P. Jönsson, X. He, C. Froese Fischer, Comput. Phys. Commun. **submitted** (2007)
30. F.A. Parpia, C. Froese Fischer, I.P. Grant, Comput. Phys. Commun. **94**, 249 (1996)
31. P. Hafner, W.H.E. Schwarz, J. Phys. B: At. Mol. Opt. Phys. **11**, 2975 (1978)
32. J. Bruneau, J. Phys. B: At. Mol. Opt. Phys. **17**, 3009 (1984)
33. I.P. Grant, Comput. Phys. Commun. **84**, 59 (1994)
34. J. Bieroń, P. Jönsson, C. Froese Fischer, Phys. Rev. A **60**, 3547 (1999)
35. J. Bieroń, P. Pyykkö, Phys. Rev. Lett. **87**, 133003 (2001)
36. K.G. Dyall, I.P. Grant, C.T. Johnson, F.A. Parpia, E.P. Plummer, Comput. Phys. Commun. **55**, 425 (1989)
37. C. Froese Fischer, T. Brage, P. Jönsson, *Computational Atomic Structure. An MCHF Approach* (Institute of Physics Publishing, London, 1997), p. 71
38. P.Å. Malmqvist, Int. J. Quantum Chem. **30**, 479 (1986)
39. J. Olsen, M.R. Godefroid, P. Jönsson, P.Å. Malmqvist, C. Froese Fischer, Phys. Rev. E **52**, 4499 (1995)
40. I.M. Savukov, W.R. Johnson, Phys. Rev. A **66**, 062507 (2002)
41. W.R. Johnson, K.T. Cheng, D.R. Plante, Phys. Rev. A **55**, 2728 (1997)
42. S.G. Porsev, A. Derevianko, Phys. Rev. A **69**, 042506 (2004)
43. P. Indelicato, F. Parente, R. Marrus, Phys. Rev. A **40**(7), 3505 (1989)
44. P. Indelicato, J.P. Desclaux, *Mcdfgme, a multiconfiguration dirac fock and general matrix elements program (release 2005)*, <http://dirac.spectro.jussieu.fr/mcdf> (2005)
45. V.A. Dzuba, V.V. Flambaum, J.S.M. Ginges, Phys. Rev. A **61**, 062509 (2000)

This figure "fig3P1.jpg" is available in "jpg" format from:

<http://arxiv.org/ps/physics/0701239v1>